Journal of Hazardous Materials 197 (2011) 285–293

Contents lists available at SciVerse ScienceDirect

Journal of Hazardous Materials

journal homepage: www.elsevier.com/locate/jhazmat

Modeling and simulation of dense cloud dispersion in urban areas by means of computational fluid dynamics

F. Scargiali, F. Grisafi, A. Busciglio, A. Brucato*

Dipartimento di Ingegneria Chimica, Gestionale, Informatica e Meccanica, Università degli Studi di Palermo, Italy

ARTICLE INFO

Article history:
Received 6 July 2011
Received in revised form
21 September 2011
Accepted 22 September 2011
Available online 29 September 2011

Keywords:
Heavy clouds
Urban canopy
CFD
Dispersion modeling
Complex terrain

ABSTRACT

The formation of toxic heavy clouds as a result of sudden accidental releases from mobile containers, such as road tankers or railway tank cars, may occur inside urban areas so the problem arises of their consequences evaluation.

Due to the semi-confined nature of the dispersion site simplified models may often be inappropriate.

As an alternative, computational fluid dynamics (CFD) has the potential to provide realistic simulations even for geometrically complex scenarios since the heavy gas dispersion process is described by basic conservation equations with a reduced number of approximations.

In the present work a commercial general purpose CFD code (CFX 4.4 by Ansys®) is employed for the simulation of dense cloud dispersion in urban areas. The simulation strategy proposed involves a *stationary pre-release* flow field simulation followed by a *dynamic after-release* flow and concentration field simulations.

In order to try a generalization of results, the computational domain is modeled as a simple network of straight roads with regularly distributed blocks mimicking the buildings. Results show that the presence of buildings lower concentration maxima and enlarge the side spread of the cloud. Dispersion dynamics is also found to be strongly affected by the quantity of heavy-gas released.

1. Introduction

Heavy clouds are gaseous mixtures of air and hazardous materials characterized by a density larger than the environment. The dispersion dynamics of such negatively buoyant mixtures can be quite different from that of neutrally or positively buoyant mixtures, depending on the initial cloud Richardson number R_{i0}, as gravity keeps them close to the ground where the threat to human safety is highest. R_{i0} is dependent on the initial cloud mass or the mass flux, the relative density excess of the cloud, the representative size of the cloud, and the ambient wind speed.

Quantitative risk analysis for loss prevention purposes demands successful simulation of possible accidental events, which is usually carried out by means of simplified empirical models. For example the so-called "box-models" developed in the past (SLAB, DEGADIS) are widely used in risk analysis procedures [1,2]. Although they show satisfactory agreement with available field observations at several sites, including some with obstacles [3] these models would have problems in areas with large terrain obstacles especially when the irregular topography of the site plays an important role [4–6]. This is the case of toxic heavy cloud formation inside urban areas, as a result of sudden accidental releases from mobile containers, such as road tankers or railway tank cars.

In this field, computational fluid dynamics (CFD) may provide the answer as it allows the simulation of complex physical processes by describing heat and mass transport phenomena with fully developed mathematical models. CFD simulations of pollutant dispersions in the atmospheric boundary layer (ABL) have been carried out in the past using the k–ε turbulence model with encouraging results both for neutrally buoyant pollutants [7] and for heavy gas dispersion processes [8–10]. Koopman and Ermak [11] reported a comprehensive review of the methodologies available to describe the dispersion of liquefied natural gas (LNG) in the ABL and stated that "Navier–Stokes models provide the most complete description of the flow and dispersion of cold, denser than air cloud in the atmosphere and are well suited for ... dispersion simulations over complex terrain".

As concerns gas dispersions in confined or semi-confined areas, CFD tools have been largely applied to describe neutrally buoyant pollutant dispersions inside urban canopies, using both RANS [12–15] and Large Eddy Simulations [16,17], or to assess a building canopy model for urban climate planning [18–20].

CFD techniques were also used to model the release and mixing process of a dense gas within buildings using RANS [5,6,21–23] and

* Corresponding author at: Dipartimento di Ingegneria Chimica, Gestionale, Informatica e Meccanica, Viale delle Scienze, Ed.6, 90128 Palermo, Italy.
Tel.: +39 09123863716; fax: +39 0917025020.
E-mail address: alberto.brucato@unipa.it (A. Brucato).

0304-3894/$ – see front matter © 2011 Elsevier B.V. All rights reserved.
doi:10.1016/j.jhazmat.2011.09.086

Nomenclature

BRFFS	Before-Release Flow Field Simulation
C_1	parameter in k–ε model (Eq. (6)), dimensionless
C_2	parameter in k–ε model (Eq. (6)), dimensionless
C_3	parameter in k–ε model (Eq. (6)), dimensionless
C_μ	constant in k–ε model (Eq. (4)), dimensionless
CRDS	Cloud Release and Dispersion Simulation
D	molecular diffusivity of chlorine in air, $m^2\,s^{-1}$
G	turbulence production due to viscous forces, $J\,m^{-3}$
G_k	turbulence production due to buoyancy forces, $J\,m^{-3}$
H	buildings height, m
IDLH	concentration "Immediately Dangerous to Life or Health", ppm
P_{ref}	reference pressure, Pa
R	ideal gas constant, $Pa\,m^3\,K^{-1}\,kmol^{-1}$
S	buildings face to face distance, m
T	temperature, K
$\mathbf{U}$	vector of velocity field, m/s
U_∞	wind velocity at 200 m above ground level, m/s
$\mathbf{U}_H$	wind velocity at top building height (H), m/s
U_x	wind velocity along wind direction (x), m/s
W	buildings width, m
M_w	mean molecular weight of the gas mixture, $kg\,kmol^{-1}$
Y	chlorine mass fraction, dimensionless
f	building fractional area coverage, dimensionless
$\mathbf{g}$	acceleration gravity, $m\,s^{-2}$
k	turbulent kinetic energy, $m^2\,s^{-2}$
p	pressure, $N\,m^{-2}$
x	distance from the release point, m

Greek symbols

ε	dissipation of turbulent kinetic energy, $m^2\,s^{-2}$
μ	viscosity, Pa s
μ_T	turbulent viscosity, Pa s
ν	kinematic viscosity, $m^2\,s^{-1}$
ν_t	turbulent kinematic viscosity, $m^2\,s^{-1}$
ρ	fluid density, $kg\,m^{-3}$
ρ_Y	dense gas density, $kg\,m^{-3}$
ρ_a	background fluid density, $kg\,m^{-3}$
σ_k	k–ε model parameters, dimensionless
σ_ε	k–ε model parameters, dimensionless
σ_Y	turbulent Schmidt number, dimensionless

LES [16,23]. Results showed reasonable agreement with flow field and gas dispersion experimental data, confirming that CFD may be an effective tool for understanding wind flow and tracer dispersion in urban areas.

The aim of the present work is that of setting up a CFD based simulation strategy for modeling dense (as well as neutrally buoyant) cloud dispersion in urban environments. The simulation strategy proposed involves a stationary pre-release flow field simulation followed by a dynamic after-release flow and concentration field simulations.

In order to generalize the results, the computational domain was modeled as a simple network of straight roads with regularly distributed blocks mimicking the buildings. Influence of building fractional area coverage and normalised height, wind velocity and release quantity on the dispersion phenomenon, was also investigated.

2. Numerical simulation

For all numerical simulations of the present work, advantage was taken from the use of the commercial CFD code CFX-4.4 by Ansys®.

2.1. Basic equations and buoyancy treatment

The simulation runs solve the Reynolds-averaged mass, momentum and scalar transport equations. If the k–ε model [24] is used for turbulence, these can be written as:

$$\frac{\partial \rho}{\partial t} = -(\nabla \cdot \rho \mathbf{U}) \tag{1}$$

$$\frac{\partial \rho \mathbf{U}}{\partial t} = -[\nabla \cdot \rho \mathbf{U}\,\mathbf{U}] - \nabla p + \nabla \cdot [\rho(\nu + \nu_t)(\nabla \mathbf{U} + (\nabla \mathbf{U})^T)] + \rho \mathbf{g} \tag{2}$$

$$\frac{\partial \rho Y}{\partial t} = -\nabla \cdot \rho \mathbf{U} Y + \rho \left(D + \frac{\nu_t}{\sigma_Y}\right) \nabla^2 Y \tag{3}$$

The turbulent kinematic viscosity ν_t is obtained from the Prandtl–Kolmogorov equation:

$$\nu_t = C_\mu \frac{k^2}{\varepsilon} \tag{4}$$

where k (turbulent kinetic energy) and ε (its dissipation rate) are computed by solving appropriate transport equations:

$$\frac{D\rho k}{Dt} = \nabla \cdot \left[\rho \left(\nu + \frac{\nu_t}{\sigma_k}\right) \nabla k\right] + \rho(G + G_k) - \rho\varepsilon \tag{5}$$

$$\frac{D\rho \varepsilon}{Dt} = \nabla \left[\rho \left(\nu + \frac{\nu_t}{\sigma_\varepsilon}\right) \nabla \varepsilon\right] + C_1 \frac{\varepsilon}{k} \rho(G + C_3 G_k) - C_2 \rho \frac{\varepsilon^2}{k} \tag{6}$$

Here, σ_k and σ_ε are turbulent Prandtl numbers for k and ε, respectively.

G is the turbulence production terms due to shear:

$$G = \rho \nu_t \nabla \mathbf{U} \cdot (\nabla \mathbf{U} + (\nabla \mathbf{U})^T); \tag{7}$$

whereas G_k is the turbulence production term associated with buoyancy. In the present case density gradients are practically entirely related to concentration gradients, as thermal gradients contribution is negligible in the relatively short (200 m) domain height. The relevant generation term was therefore computed as:

$$G_k = -\frac{\nu_t}{\sigma_k} g \nabla \rho = -\frac{\nu_t}{\sigma_k} \alpha \rho_a g \nabla Y \tag{8}$$

where $\alpha = (\rho_Y - \rho_a)/\rho_a$ is a density coefficient due to concentration, ρ_Y and ρ_a being the densities of the dense gas and background fluid, respectively.

The parameter values used in all simulations are the "consensus" values for k–ε model:

$$C_\mu = 0.09; \quad C_1 = 1.44; \quad C_2 = 1.92; \quad C_3 = 0.50; \quad \sigma_k = 1.0;$$

$$\sigma_\varepsilon = 1.3$$

The so-called *weakly compressible* approximation (CFX 4.4 User Manual) was adopted for the buoyancy treatment instead of the simpler Boussinesq approximation employed elsewhere [8], in view of the strong density gradients in the proximities of the dense plume. The main hypothesis behind this approximation is that density variations are related only to the mean molecular weight and/or temperature changes in the fluid, while density is assumed to be independent of the pressure field. Density is in practice expressed by the following equation of state:

$$\rho = \frac{P_{ref} M_w}{RT} \tag{9}$$

Hence a constant reference pressure is assumed for the estimation of fluid density; as a consequence, no sound waves are possible (*i.e.*

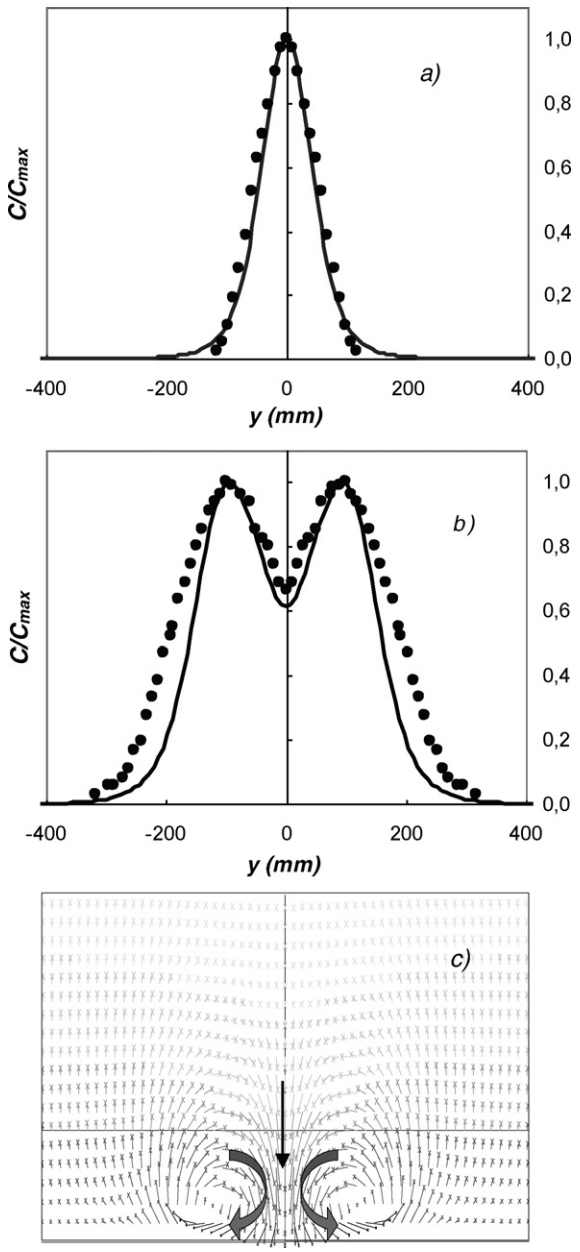

Fig. 1. Simulation and experiment for the release of continuous plumes: (a) neutrally buoyant plume ($\rho/\rho_{env} = 1$); (b and c) dense plume ($\rho/\rho_{env} = 2$); (a and b) horizontal mean concentration profiles on a transversal line 0.5 m downwind the release point: symbols: experimental data by Ayrault et al. [26]; solid lines: CFD simulation results [25]; (c) dense plume vector plot over a vertical-transversal plane 0.1 m downwind the release point [25].

sound speed is infinite). The reference pressure P_{ref} was always set at 1 atm in the present case.

The dense gas dispersion model here adopted has already been validated [25] by comparison with the literature experimental data. The simulations there performed concerned the experiments carried out by Ayrault et al. [26], involving either neutrally buoyant or heavy continuous plume releases in an atmospheric wind tunnel. Simulations were found to correctly predict the switch from the Gaussian profile characterizing neutrally buoyant dispersions (Fig. 1a) and the bi-modal pattern experimentally observed with negatively buoyant plumes (Fig. 1b) over a detection line placed 100 mm downstream a transverse solid fence obstacle 30 mm high. The latter feature of the concentration field is related the appearance of two counter-rotating vortexes (Fig. 1c) generated by density gradient gravitational effects that are not found in the case of neutral release. The good agreement between simulation results and experiment can clearly be regarded as a confirmation of the overall soundness of the model here adopted.

3. Simulation strategy

3.1. Simulation strategy and computational details

The computational domain was modeled as a simple network of straight roads with regular blocks mimicking the buildings. The release point was placed in the middle of a crossing, as depicted in Fig. 2.

Buildings height, width, and face to face distance were varied in order to assess their influence on the dispersion process. The total computational grid encompassed about 700,000 cells to guarantee a fine discretization between the buildings. In the vertical direction, grid cells were clustered close to the ground, to improve discretization where needed.

The simulation of each release event was conducted in two steps: (i) the first step was devoted to the generation of the flow field before the release, while the second step (ii) dealt with the after-release heavy cloud dispersion, as detailed in the next two sections.

3.2. Before-Release Flow Field Simulation (BRFFS)

Having split the simulation in two steps, the stationary pre-release flow field was conveniently computed by carrying out a "steady-state" simulation, with large savings of CPU time with respect to a dynamic simulation carried on until steady state convergence. Moreover, the simulated system consisted of an indefinitely wide network of buildings separated by straight roads. As such the physical system considered is characterized by periodicities along both roads directions. As a consequence, in order to obtain the before-release flow field in the indefinitely wide buildings network, simulations could be limited to a much smaller domain surrounding a single building, by suitably imposing periodic boundary conditions on all four lateral vertical planes, as depicted in Fig. 2. The computational grid adopted encompassed $26 \times 26 \times 45 = 30{,}426$ cells and is reported in Fig. 3. A constant wind speed (7 m/s in most cases) was imposed at the top boundary of the domain, 200 m above ground level.

In this way the pre-release turbulent flow field obtained does include the mechanical turbulence generation due to terrain geometry while turbulence generation/suppression effects by thermal gradients (related to air stability classes) are not considered. In practice the simulations performed concern stable atmospheric boundary layer (ABL) conditions. As a matter of fact, mechanical turbulence generation should be expected to be the major turbulence source at the investigated system scales, while the (larger scale) turbulence generated by thermal gradients inside the (much higher) ABL can be expected to be less important.

An examples of vector plot obtained on a vertical plane across the buildings is reported in Fig. 4 where the presence of a flow recirculation vortex between subsequent buildings is evident.

Pre-release flow field simulation results were quantitatively compared with experimental data available in the literature [27]. In Fig. 5a and b experimental vertical profiles of normalised horizontal velocity (U_x) obtained behind a building (point A in the figure) and in the gap between buildings (point B in the figure) are compared with the relevant simulation results. As it can be seen, the simulated before-release flow-field (solid lines), is in good agreement with experiment (symbols) with a maximum standard deviation of 6%. This implies that the computational options here adopted are adequate for the present simulation purposes.

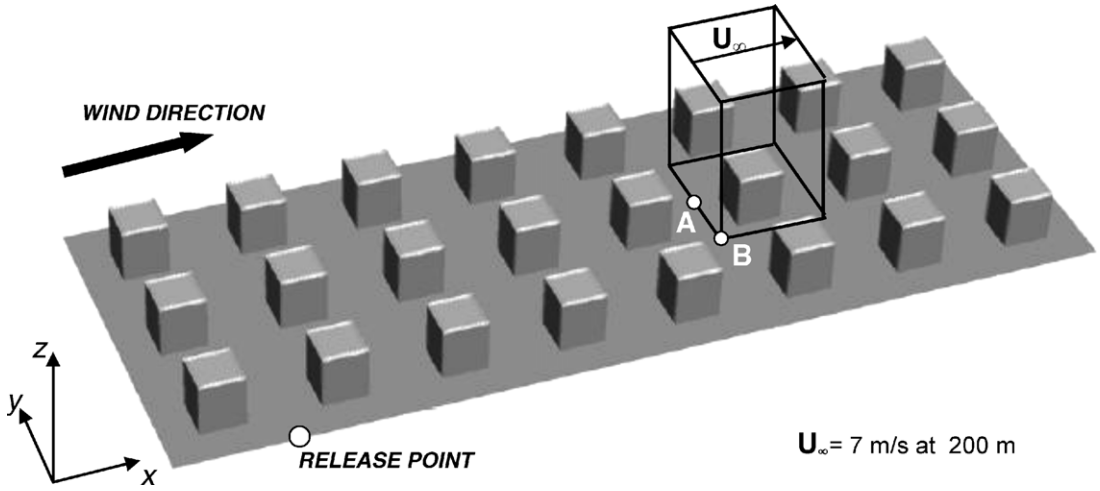

Fig. 2. Sketch of the computational domain. The box represents the computational domain used for the "*Before Release Flow Field Simulations*" (BRFFS).

3.3. Cloud Release and Dispersion Simulation (CRDS)

After the release, the presence of the heavy cloud is bound to significantly affect the local flow field (as witnessed by Fig. 1), and this changes in time while cloud size, shape and concentration change, due to convection and dispersion phenomena. As a consequence the flow field undergoes a time dynamics, which has to be accounted for if realistic simulations are to be carried out. To this end fully time dependent flow field simulations were carried out in conjunction with cloud scalar transport simulations.

In practice the flow, pressure and turbulence fields predicted in the first step of the simulation strategy around the generic building, were imposed as initial conditions around each of the 24 buildings of the new computational domain (see Fig. 1). At the upstream vertical boundary the relevant velocities and turbulence quantities computed in the first step were adopted as stationary inlet conditions.

At the two lateral vertical sides of the domain, symmetry conditions were specified, which constrained the bulk flow to be parallel to the lateral boundaries at the locations. At the upper surface of the domain, quite far away from ground level, a symmetry condition was also specified, to ensure that velocity stayed horizontal throughout the simulation and that all quantities had zero gradients across the boundary.

All the above boundary conditions derive in practice from the reasonable assumption that boundaries were sufficiently far away from the cloud region for possible boundary condition oversimplifications to negligibly affect simulation results.

Finally, no-slip conditions were imposed at all bottom and building walls, while at the downstream boundary a "mass flow" boundary condition was specified, which fixes the total mass outflow to be the same as that entering the domain from all sources.

The flow field simulations of the after-release cloud dispersion process were carried out in transient conditions until the gas cloud had exited the computational domain. The time step was chosen in such a way that in all cells a Courant number (defined as the ratio between simulation time step and the fluid flight time over the cell) smaller than one was obtained. The differentiation scheme adopted

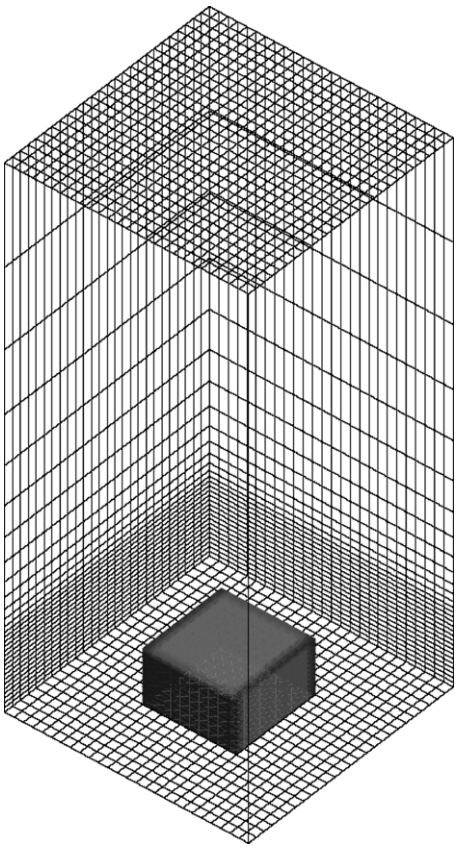

Fig. 3. Computational domain for the "*Before Release Flow-Field Simulations*" (BRFFS).

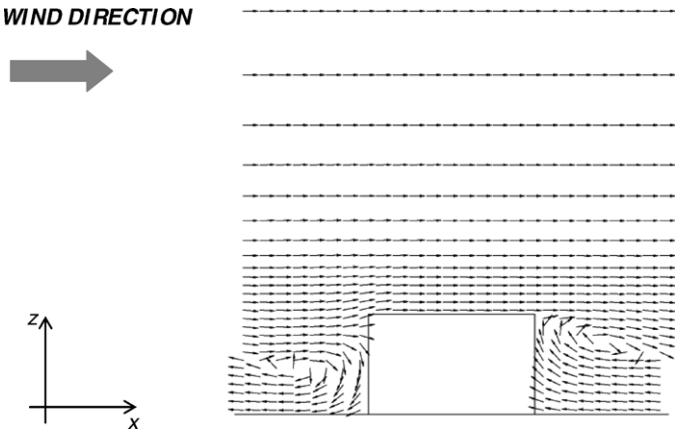

Fig. 4. Vector plot on a vertical plane, across a building and parallel to wind direction (all vectors sharing the same size in order to highlight flow structure).

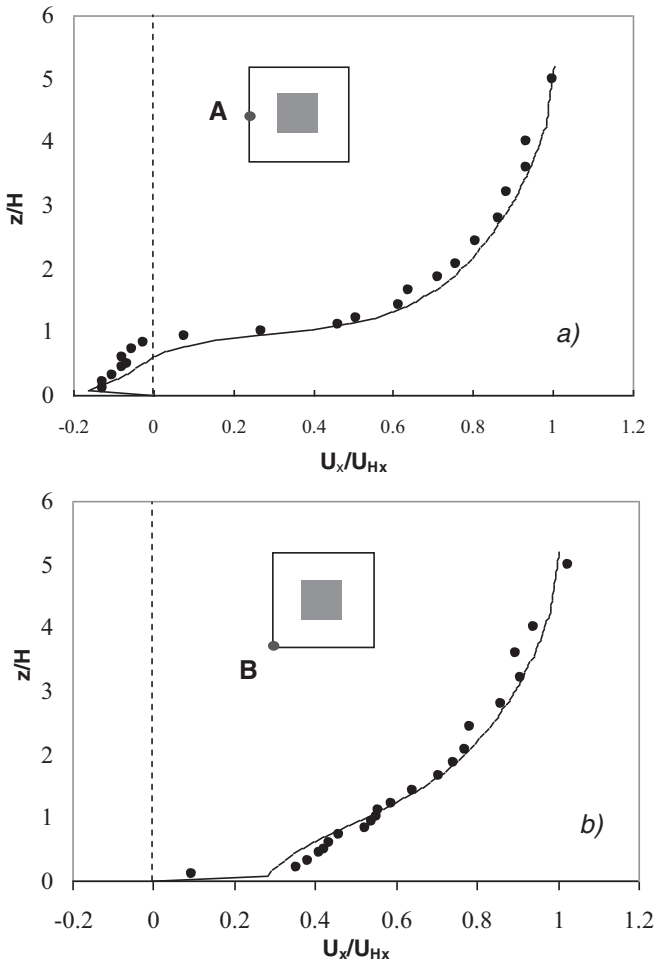

Fig. 5. Vertical profiles of normalised velocity (U_x/U_{Hx}) in the wake (a), and in the gap (b): • experimental data; – model data.

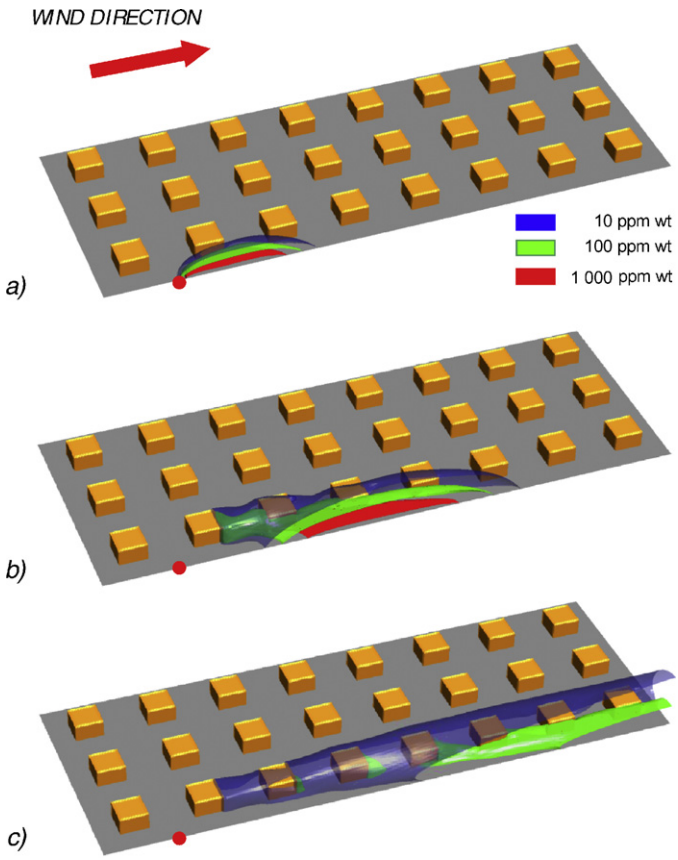

Fig. 6. Constant chlorine concentration isosurfaces for case 1 (*base case*), 15 s (a), 60 s (b) and 180 s (c) after the release.

was the (mainly second order) *hybrid up-wind* for all computed quantities.

The 11 test cases analysed are listed in Table 1. Buildings height (H), width (W), and face to face distance (S), were varied from run to run in order to evaluate the influence of these parameters on the dispersion phenomenon (cases 1–5). Two further scenarios, simulated only for comparison purposes, regarded the assumption of flat terrain (case 6) and the release of a neutrally buoyant gas (case 11).

For the cloud dispersion simulations a certain amount of chlorine was assumed to be suddenly released inside the computational domain. In most cases, the instantaneous quantity of chlorine released was assumed to be about 90 kg. In order to assess the influence of released quantity on dispersion dynamics, also the cases of ten times smaller (case 7) and larger (case 8) releases were considered. In all cases the release point was assumed to be placed in the middle of the crossing at zero meters above ground.

Strong simplifications were made as regards the simulation of the complex physicochemical phenomena involved in the initial seconds of the release, as jet dispersion, temperature variations, presence of liquid drops, etc. were neglected. In practice, the entire quantity released was assumed to immediately assume the temperature and velocity of air in the cells of emission (as obtained in the first step of the simulation work). In the base case (case 1 in Table 1) it was assumed that the release resulted in instantaneously filling a volume of 4 m × 4 m × 2 m (x, y, z directions, respectively) so resulting in a release of 90.7 kg of chlorine. For the larger release case (case 8) it was assumed that the volume entirely filled was 8 m × 8 m × 5 m (x, y, z directions, respectively) hence resulting in a release of 907 kg of chlorine, while for the smaller release case (case 7), it was assumed that a volume of 2 m × 4 m × 1 m (1 × 2 × 1 cells in the x, y, z directions, respectively) was filled with a gas mixture containing 61 wt.% of chlorine, hence resulting in a release of 9.02 kg of chlorine. The above simplifications were considered acceptable in the present work especially in view of the simulation runs purpose, *i.e.* studying the influence of buildings and streets geometry on heavy gas dispersion dynamics in urban environment.

Finally the influence of wind velocity on the heavy cloud dispersion dynamics was analysed in cases 9 and 10 where a wind speed of, respectively, 3.5 m/s and 14 m/s at 200 m above ground was imposed.

4. Results and discussion

4.1. Heavy-gas dispersion: influence of geometrical parameters

The simulation results obtained for the base case (case 1 in Table 1) are reported in Fig. 6 as three-dimensional views of chlorine concentration *isosurfaces* at 15, 60 and 180 s after the release. The outer *isosurface* (coloured in blue) refers to a chlorine concentration in air of 10 ppm wt. (For interpretation of the references to colour in text, the reader is referred to the web version of this article.) This surface may be regarded as a safe external cloud boundary in view of the reference concentration of about 25 ppm wt, which is currently considered as “Immediately Dangerous to Life or Health” (IDLH) by the *NIOSH* [28]. Two other *isosurfaces* (visible in lighter green and red colours), corresponding to 100 and 1000 ppm wt, are represented inside the cloud boundary to highlight the width

Table 1
Cases analysed.

Case	Quantity released (kg)	Initial cloud size (m^3)	ρ/ρ_{env}	H (m)	S (m)	W (m)	U_∞ (m/s) (200 m height)	H/W	f % fract. area coverage
1 (Base)	90.7	34	2.45	12	32	20	7.0	0.6	15
2	90.7	34	2.45	**6**	32	20	7.0	**0.3**	15
3	90.7	34	2.45	**24**	32	20	7.0	**1.2**	15
4	90.7	34	2.45	12	**48**	20	7.0	0.6	**9**
5	90.7	34	2.45	12	**24**	20	7.0	0.6	**21**
6 (Flat terrain)	90.7	34	2.45	**0**	∞	**0**	7.0	**0**	**0**
7	**9.02**	**3.4**	2.45	12	32	20	7.0	0.6	15
8	**907**	**344**	2.45	12	32	20	7.0	0.6	15
9	90.7	34	2.45	12	32	20	**3.5**	0.6	15
10	90.7	34	2.45	12	32	20	**14.0**	0.6	15
11 (Neutrally buoyant cloud)	90.7	34	**1**	12	32	20	7.0	0.6	15

of strongly affected areas as well as the intensity of gradients in the proximity of cloud boundary.

As it can be seen, shortly after the release (Fig. 6a), the cloud has a flat and rounded shape, as it is typical of heavy clouds. After the first minute (Fig. 6b) while the higher concentration *isosurface* (1000 ppm) has already reached the third street crossing, part of the cloud is still trapped between the first buildings, where the presence of recirculation vortices slows down cloud dispersion. After 3 min (Fig. 6c), the cloud core has already passed through the computational domain, though zones with a chlorine concentration higher than the IDLH are still present in side streets.

For comparison purposes, the dispersion of a neutrally buoyant cloud (case 11) is presented in Fig. 7a–c. All computational parameters were set identical to "case 1", with the exception of cloud density, which was imposed to be the same as that of surrounding air. As it can be seen the simulated dispersion process is rather

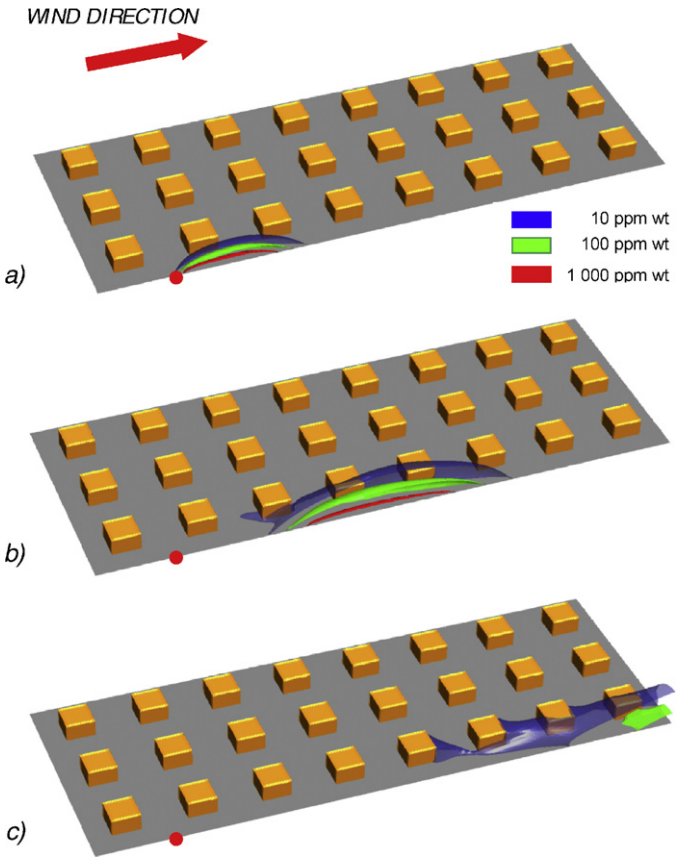

Fig. 7. Constant chlorine concentration isosurfaces for case 11 (*neutrally buoyant cloud*), 15 s (a), 60 s (b) and 180 s (c) after the release.

different from that reported in Fig. 6a–c, which confirms the importance of buoyancy effects for the dispersions under investigation. In particular the *isodense* cloud has a more regular shape and the presence of buildings has a lower influence on cloud dispersion process, leaving the cloud freer to move along wind direction (compare Figs. 6b and 7b). Also the cloud moves faster and after 3 min the cloud has almost completely left the computational domain (Fig. 7c).

The influence of buildings height is shown in Fig. 8a–d, where cloud boundaries 30 s after the release, are shown for flat terrain and three different building heights (cases 6, 2, 1 and 3, respectively). The ratio between buildings height (H) and buildings width (W) is used as non-dimensional parameter. As it can be seen, in the case of flat terrain the cloud is flatter and longer and it is moving faster than in the other cases along the wind direction. The buildings presence clearly induces larger vertical and lateral dispersions, also slowing down the cloud.

In order to get a quantitative appreciation of the diverse dispersion conditions, in Fig. 9 maxima of the chlorine mass fraction on the ground are reported versus downwind distance (for the same cases already shown (cases 1, 2, 3 and 6)). For each location downwind the release point, the value reported here is the highest ground-level chlorine mass fraction experienced by that location during the entire dispersion process. In practice, each curve reported in Fig. 9 may be regarded as the envelope of all instantaneous spatial distributions of the ground-level chlorine mass fraction distributions. It is possible to observe that the C_{max} achieved at the various distances decreases when buildings height increases, which is clearly a consequence of the vertical dispersion induced by the buildings. It is worth noting that the first two curves, pertaining to flat terrain and 6 m high buildings do practically coincide, which implies that in order for the building dispersive effects to become important, a minimum building height is needed. Notably, the same chlorine concentration maximum is achieved for the two cases at different times after the release, as it can be inferred by comparing Figs. 8 and 9.

From what proceeds it may be stated that, using a flat terrain simplified model may be appropriate for relatively short houses and will result into conservative estimates in the case of taller buildings. On the other hand, a flat terrain simplified model would never be able to highlight the presence of dangerous concentration of heavy gas in lateral streets.

The results obtained when varying the building fractional area coverage "f":

$$f = \frac{W^2}{(W+S)^2} \tag{10}$$

are reported in Fig. 10, where the maximum concentrations reached at fixed times after the release are reported as a function of the relevant distances downstream the release point for the flat terrain case ($f = 0$), case 1 ($f = 0.15$), case 4 ($f = 0.09$) and case 5 ($f = 0.21$). The effect

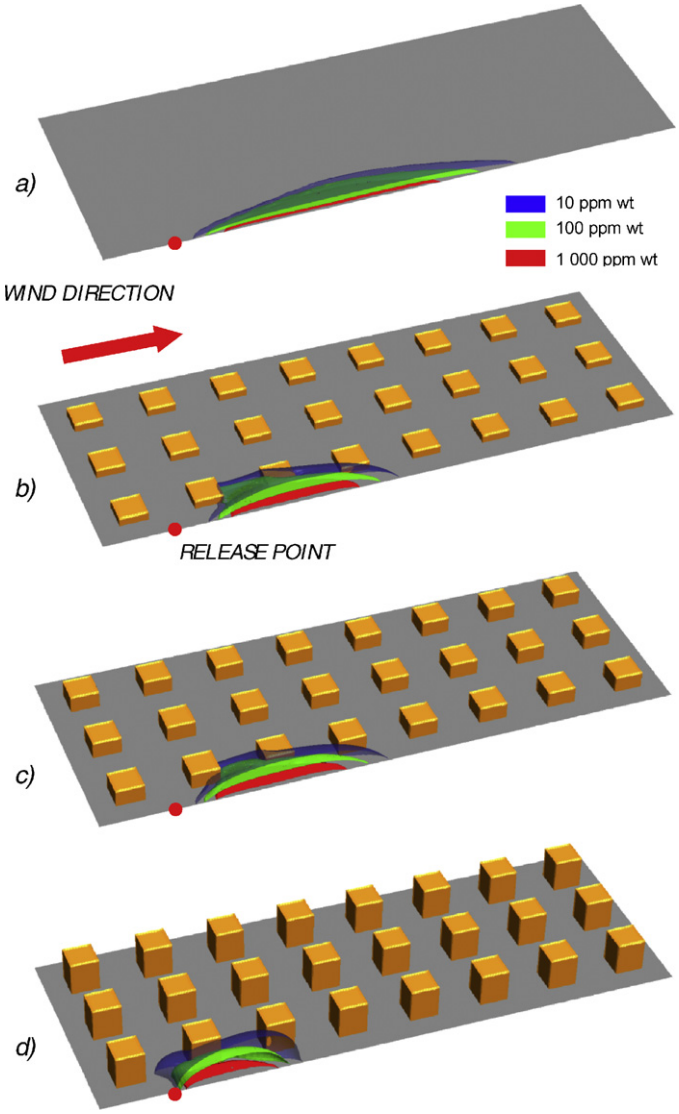

Fig. 8. Constant chlorine concentration isosurfaces for different building heights (H), 30 s after the release: (a) flat terrain (case 6); (b) H = 6 m (case 2); (c) H = 12 m (case 1); (d) H = 24 m (case 3).

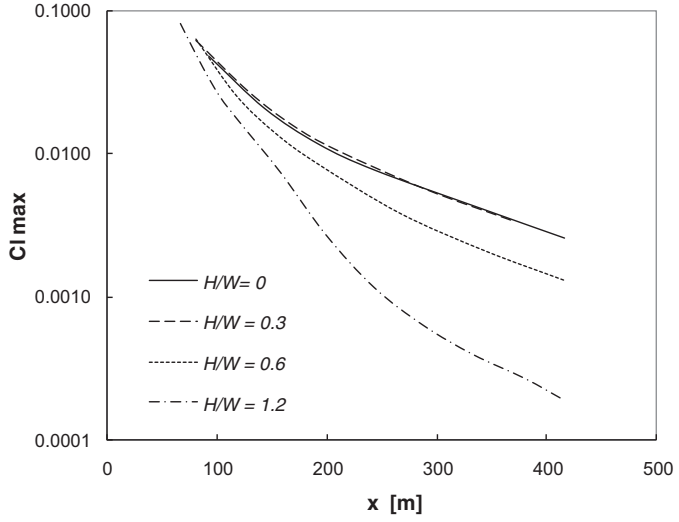

Fig. 9. Influence of normalised buildings height on the maximum concentrations achieved versus relevant distances from the release point.

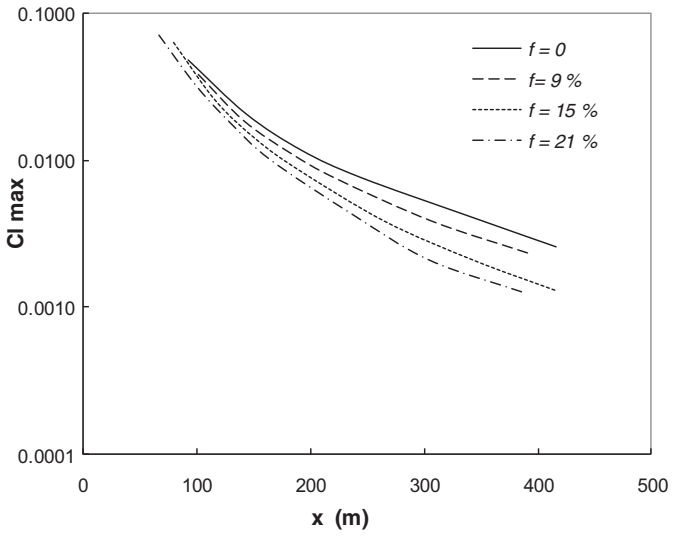

Fig. 10. Influence of buildings fractional area coverage on the maximum chlorine concentrations achieved versus relevant distances from the release point.

of buildings is again that of increasing cloud lateral spread while the distance between buildings gets shorter. This effect contributes to faster dispersion, as it can be appreciated in Fig. 11.

4.2. Influence of wind speed

Cases 9 and 10 of Table 1 regarded the same geometrical conditions and released quantity as in the base case, but different wind speeds 200 m above ground level (3.5 and 14 m/s, respectively). Of course, heavy cloud advancing velocity increases when wind speed increases, and the maximum concentration reached at the given times strongly decreases as wind speed is increased, as shown in Fig. 11a, due to the larger distance travelled by the cloud. It is worth noting that if one reports maximum chlorine concentrations at ground level versus the relevant distances from the release point (Fig. 11b) the three curves tend to collapse on a single line, which implies that the dispersion phenomena occurring are mainly based on convective effects. These are related to average velocities, which are essentially proportional to the forcing wind. As a consequence a faster forcing speed substantially results in the same sequence of pictures, but occurring at a faster pace.

4.3. Influence of released gas quantity

The characteristic behaviour of heavy clouds and their tendency to stratification during the dispersion process strictly depends on cloud mixture density. As cloud density decreases when air is mixed in, buoyancy effects decrease until cloud density becomes practically equal to environment density. For this reason, though starting from the same initial concentration, a larger quantity of mass released may be expected to experience a slower dilution than a small quantity so maintaining a "negatively buoyant" behaviour for a longer time. In Fig. 12a, b and c three different chlorine concentration contours on the ground, normalised with respect to the amount released are plotted 30 s after the release, for the same geometry parameters and wind speed. For comparison purposes, in Fig. 12d normalised concentration contours for a "*neutrally buoyant*" gas release are reported. The three dense gas releases differ only in the total released mass (9, 90, and 900 kg) and are otherwise identical. If the released gas were neutrally buoyant, its mass fraction would be a purely passively advected scalar; its spatial distribution would be strictly proportional to the total quantity

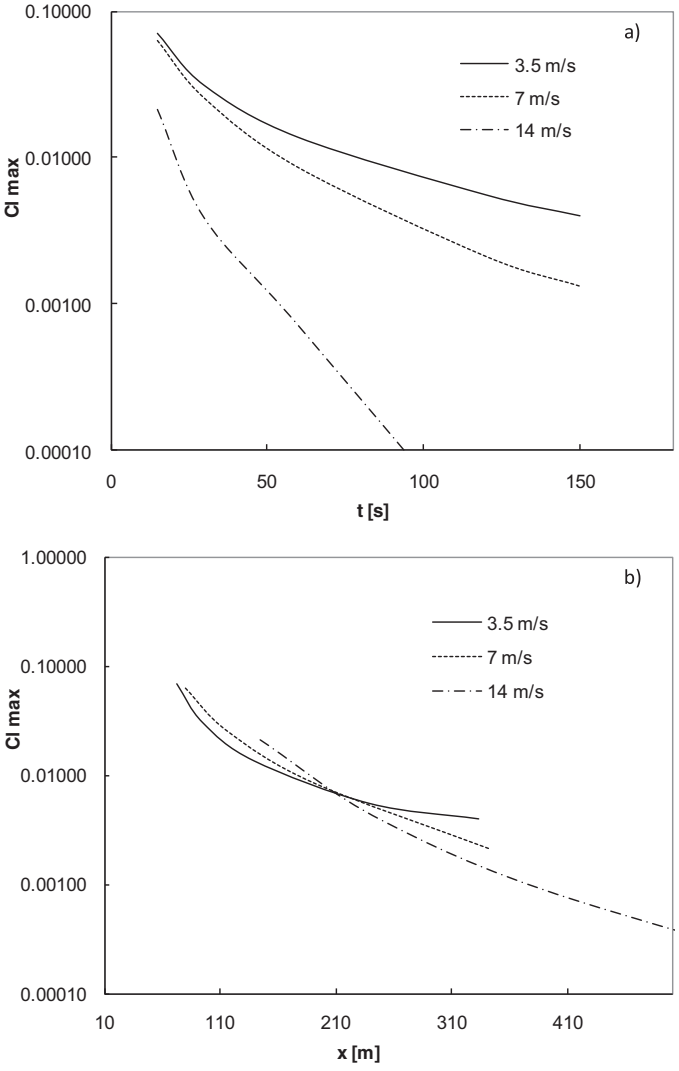

Fig. 11. Influence of wind speed on maximum chlorine concentration at ground level: (a) maximum chlorine mass fraction attained at relevant time instants; (b) maximum chlorine mass fraction versus relevant distances from the release point. Solid line, U_∞ = 3.5 m/s; dashed line, U_∞ = 7.0 m/s; dash-dotted, U_∞ = 14.0 m/s.

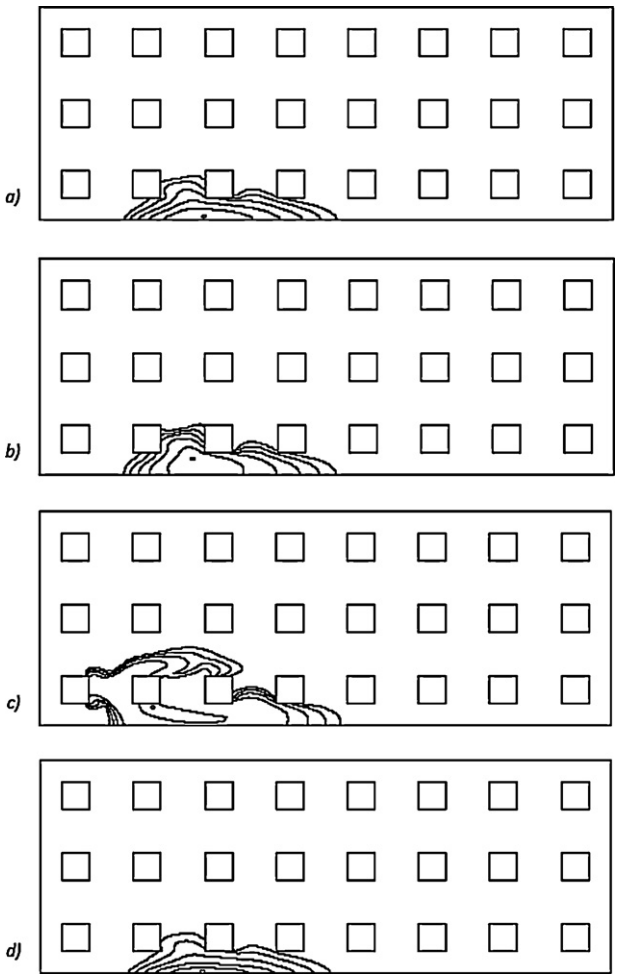

Fig. 12. (a, b and c) Chlorine normalised contours 30 s after the release. Quantity released: (a) 9 kg; (b) 90 kg; (c) 900 kg; chlorine contours: (a) 0.1, 10, 100, 1000 ppm wt; (b) 1, 10,100, 1000, 10,000 ppm wt; (c) 10, 100, 1000, 100,000 ppm wt, innermost circle: location of chlorine maximum concentration. (d) Neutrally buoyant gas normalised contours 30 s after the release. Quantity released: 90 kg; contours: 1, 10,100, 1000, 10,000 ppm wt. Grey circle: location of chlorine maximum concentration.

released and the three normalised contours reported in Fig. 12a, b and c would exhibit exactly the same shape.

Actually, the normalised contours are significantly different from each other, especially for the largest release (Fig. 12c, 900 kg) where the lateral dispersion of the cloud is much higher than in the other cases, with the cloud reaching also the nearby parallel street while the vertical dispersion is lower. Notably, the concentration maximum (innermost circle in Fig. 12), that lays on the symmetry axis in the case of a neutrally buoyant release (Fig. 12d), is never on the symmetry axis for the heavy releases (thus implying bimodal concentration profiles similar to that in Fig. 1b), with the displacement from the symmetry axis increasing while the amount released increases. It is worth noting that the smaller heavy gas release of 9 kg (Fig. 12a) behaves almost as a neutrally buoyant cloud as it is possible to appreciate by comparing Fig. 12a and d.

The above results show that it is not possible to perform a simulation with a reference amount released and then to extend the results obtained to all possible scenarios by simply setting a constant concentration-multiplier proportional to the amount released. This makes any quantitative generalization of results very hard if not impossible. On the other hand, results from the present study should help getting a perception of the sensitivity of dispersion features to the main parameters affecting the dispersion, and highlighting the differences that should be expected from the much simpler case of heavy releases over a flat terrain, for which simple models are available in the literature.

5. Conclusions

A two-step simulation procedure for the dense cloud dispersion able to exploit general purpose CFD codes has been developed and applied to a simplified geometry mimicking an infinitely wide urban canopy. The main novelty of the proposed simulation strategy lies on the fact that simulations were carried out in two steps.

The first step, *Before-release flow field simulation* (*BRFFS*), was aimed at computing the stationary flow and turbulence fields existing before the release. To this end a suitable three-dimensional generalized "box" representing a generic building surrounded by straight roads inside the urban area was numerically simulated while imposing steady-state conditions. The before-release flow fields obtained were found to be in good agreement with the literature experimental data.

In the second step, *Cloud Release and Dispersion Simulation* (*CRDS*), the dispersion of a heavy cloud (chlorine gas) released inside the computational domain was simulated with proper boundary conditions as assessed in the first step. Also, a suitable

scalar transport equation was added to the purely thermo-fluid-dynamics equations and the so-called "weakly compressible" approximation was adopted to account for the density effects associated with gas concentration.

Results confirm that the presence of buildings reduces maximum ground concentrations while enlarging the affected area interested. Due to the larger negative buoyancy effects, increasing the amount of heavy-gas released slows down the cloud and increases (normalised) maximum concentrations and lateral spread of the cloud.

The approach proposed in this work may be employed to help setting up and validating simplified dispersion models by providing the information needed to asses the dependence of heuristic model parameters on the main geometric features of urban areas.

Acknowledgment

This research work was carried out under financial support by University of Palermo.

References

[1] S.R. Hanna, D. Strimaitis, Workbook of Test Cases for Vapour Cloud Source Dispersion Models, Center for Chemical Process Safety, AIChE, New York, 1989.
[2] F. Rigas, M. Konstandinidou, P. Centola, G.T. Reggio, Safety analysis and risk assessment in a new pesticide production line, J. Loss Prev. Process Ind. 16 (2003) 103–109.
[3] R.S. Hanna, J.C. Chang, Use of the Kit Fox field data to analyze dense gas dispersion modelling issues, Atmos. Environ. 35 (2001) 2231–2242.
[4] N.J. Duijm, B. Carissimo, A. Mercer, C. Bartholomè, H. Giesbrecht, Development and test of an evaluation protocol for heavy gas dispersion models, J. Hazard. Mater. 56 (1997) 273–285.
[5] M.A. McBride, M.D. Reeves, M.D. Vanderheyden, C.J. Lea, X.X. Zhou, Use of advanced techniques to model the dispersion of chlorine in complex terrain, Trans. IChemE, Part B, Process Saf. Environ. Protect. 79 (B2) (2001) 89–102.
[6] S. Sklavounos, F. Rigas, Simulation of Coyote series trials – part I: CFD estimation of non-isothermal LNG releases and comparison with box-model predictions, Chem. Eng. Sci. 61 (2006) 1434–1443.
[7] A. Huser, P.J. Nilsen, H. Skatun, Application of k–ε model to the ABL: pollution in complex terrain, J. Wind Eng. Ind. Aerodyn. 67–68 (1997) 425–436.
[8] F. Scargiali, E. Di Rienzo, M. Ciofalo, F. Grisafi, A. Brucato, Heavy gas dispersion modelling over a topographically complex mesoscale: a CFD based approach, Trans. IChemE, Part B, Process Saf. Environ. Protect. 83 (B3) (2005) 242–256.
[9] I.V. Kovalets, V.S. Maderich, Numerical simulation of interaction of the heavy gas cloud with the atmospheric surface layer, Environ. Fluid Mech. 6 (2006) 313–340.
[10] A. Luketa-Hanlin, R.P. Koopman, D.L. Ermak, On the application of computational fluid dynamics codes for liquefied natural gas dispersion, J. Hazard. Mater. 140 (2007) 504–517.
[11] P.R. Koopman, D.L. Ermak, Lessons learned from LNG safety research, J. Hazard. Mater. 140 (2007) 412–428.
[12] J.J. Baik, J.J. Kim, On the escape of pollutants from urban street canyons, Atmos. Environ. 36 (2002) 527–536.
[13] M. Schatzmann, B. Leitl, Validation and application of obstacle-resolving urban dispersion models, Atmos. Environ. 36 (2002) 4811–4821.
[14] J.J. Kim, J.J. Baik, Effects of inflow turbulence intensity on flow and pollutant dispersion in an urban street canyon, J. Wind Eng. Ind. Aerodyn. 91 (2003) 309–329.
[15] I.R. Cowan, I.P. Castro, A.G. Robins, Numerical considerations for simulations of flow and dispersion around buildings, J. Wind Eng. 67–68 (1997) 535–545.
[16] A. Walton, A.Y.S. Cheng, Large-eddy simulation of pollution dispersion in an urban street canyon – part II: idealised canyon simulation, Atmos. Environ. 36 (2002) 3615–3627.
[17] R.F. Shi, Z.S. Cui, Z.S. Wang, Z.S. Xu, Z.S. Zhang, Large eddy simulation of wind field and plume dispersion in building array, Atmos. Environ. 42 (2008) 1083–1097.
[18] Y. Ashie, V.T. Ca, T. Asaeda, Building canopy model for the analysis of urban climate, Atmos. Environ. 81 (1999) 237–248.
[19] E.R. Marciotto, A.P. Oliveira, S.R. Hanna, Modelling study of the aspect ratio influence on urban canopy energy fluxes with a modified wall-canyon energy budget scheme, Build. Environ. 45 (2010) 2497–2505.
[20] R.A. Memon, D.Y.C. Leung, C.H. Liu, Effects of building aspect ratio and wind speed on air temperature in urban-like street canyons, Build. Environ. 45 (2010) 176–188.
[21] S. Gilham, D.M. Deaves, P. Woodburn, Mitigation of dense gas releases within buildings: validation of CFD modelling, J. Hazard. Mater. 71 (2000) 193–218.
[22] S. Sklavounos, F. Rigas, Validation of turbulence models in heavy gas dispersion over obstacles, J. Hazard. Mater. A108 (2004) 9–20.
[23] S.R. Hanna, M.J. Brown, F.E. Camelli, S.T. Chan, W.J. Coirier, O.R. Hansen, A.H. Huber, S. Kim, R.M. Reynolds, Detailed simulations of atmospheric flow and dispersion in downtown Manhattan, Bull. Am. Meteorol. Soc. 12 (2006) 1713–1726.
[24] B.E. Launder, D.B. Spalding, The numerical computation of turbulent flows, Comput. Meth. Eng. 3 (1974) 269–289.
[25] F. Scargiali, F. Grisafi, G. Micale, A. Brucato, CFD simulation of dense plumes in an atmospheric wind tunnel, in: Proc. LP 2004, Praha, Czech Republic, 31 May–3 June, 2004, ISBN 80-02-01574-6, pp. 3137–3142.
[26] M. Ayrault, S. Simoëns, P. Méjean, Negative buoyancy effects on the dispersion of continuous gas plumes downwind solid obstacles, J. Hazard. Mater. 57 (1998) 79–103.
[27] S.R. Hanna, S. Tehranian, B. Carissimo, R.W. Macdonald, R. Lohner, Comparison of model simulations with observations of mean flow and turbulence within simple arrays, Atmos. Environ. 36 (2002) 5067–5079.
[28] U.S. National Institute for Occupational Safety and Health, NIOSH Pocket Guide to Chemical Hazards, J.J. Keller and Associates, Inc., USA, 1997.